

---

---

# Enhanced Imagery Using Spectral-Estimation-Based Techniques

Thomas G. Moore, Brian W. Zuerndorfer, and Earl C. Burt

■ Since the early 1970s, Lincoln Laboratory has been working on algorithms to enhance the resolution of imagery from wideband radars. This article describes a class of algorithms that are based on the technique of bandwidth extrapolation, which uses a model-based spectral-estimation technique for generating synthetic radar data. The extrapolated radar data are combined with the measured radar data in a Fourier transform to produce images with high spectral resolution. The article describes the application of these algorithms to measured radar data from a small commercial aircraft in flight.

**I**NVERSE SYNTHETIC-APERTURE radar, or ISAR, promises to provide a rich collection of features for identifying targets such as satellites, aircraft, and ground vehicles at very long ranges. To fulfill this promise, the target imagery must have adequate resolution to isolate distinct portions of the target. The creation of high-resolution ISAR imagery requires two important elements: wideband processing for resolution in range and relatively long integration times for resolution in cross-range.

Since 1979, the Radar Imaging Techniques group at Lincoln Laboratory has used ISAR image processing to perform space object identification in support of the U.S. Space Command and the U.S. Air Force Space Command. The radars used for this surveillance have range resolutions varying from 50 cm to 13 cm. Because the orbital motion of most satellites can be well characterized, we can process the radar data to achieve cross-range resolutions comparable to or better than range resolutions.

In recent years there has been a trend to reduce the number of functions a satellite performs and thereby reduce its size, which in turn reduces launch costs. This trend poses a challenge for the space-surveillance mission. As satellites become smaller, the correspond-

ing need for higher image resolution to perform the surveillance mission becomes greater. The enormous cost of procuring a new wideband radar is a significant incentive to combine modern signal processing techniques with current radar equipment to yield high-resolution imagery with equivalent bandwidth.

Another area of research is the use of wideband radars for noncooperative target identification in support of past and current research efforts at Wright Laboratory [1]. The work for Wright Laboratory involves applying bandwidth-extrapolation techniques to solve some of the problems that occur in wideband air-to-air combat identification techniques. Current multifunction radars often have limited available bandwidth and can have difficulty dedicating the long uninterrupted integration periods required for high-resolution processing. As a result, there are four constraints on the collection of data used for ISAR imagery: (1) only moderate bandwidths may be achievable, (2) portions of the signal band may be unusable because of signal interference even if adequate bandwidths can be achieved, (3) data integration periods may be shorter than required, and (4) pulses may be missing because of contention with other critical radar activities such as search and target

track. In addition, the amount of time the processor requires to produce the required resolution may be too long for the real-time tracker to produce a well-focused image.

Since the early 1970s, Lincoln Laboratory has been working on signal processing techniques for improving radar image formation [2, 3]. We have developed robust processing techniques for enhancing range resolution to support analysis of ISAR imagery of satellites, strategic targets, and aircraft. The original work on bandwidth extrapolation was performed by S.B. Bowling [4] in the late 1970s. More recently the bandwidth-extrapolation technique was revived by K.M. Cuomo [5]. The authors of this article have been applying the technique to the imaging of satellites and aircraft since 1991 [6, 7]. This article provides a concise summary of the results we achieved and the lessons we learned during that period.

In the sections that follow, we present the theory of bandwidth extrapolation, aperture extrapolation, and bandwidth interpolation as developed for enhancing ISAR image resolution in both range and cross-range. We then present some specific examples of resolution enhancement in both range and cross-range.

### Theory

In using wideband-radar data for imaging, we require sufficient resolution to distinguish prominent portions of the target. Resolution is commonly obtained through conventional Fourier processing and is limited in range by the bandwidth of the radar and in cross-range by the temporal duration of radar pulse integration. In the class of techniques referred to as bandwidth extrapolation, aperture extrapolation, and bandwidth interpolation, a mathematical model based on the physics of high-frequency scattering of the target is fitted to the radar data. The information gained from this modeling is then used in bandwidth extrapolation to enhance resolution, in aperture extrapolation to enhance cross-range resolution and increase image focusing, and in bandwidth interpolation to repair spectral or pulse-collection gaps.

#### Background

At high frequencies, where the dimensions of the target are typically large compared to the radar wave-

length, the radar cross section  $\sigma$  produced by a target is given by  $\sigma = \|V(f)\|^2$ , where the complete frequency response  $V(f, \theta)$  of the target is

$$V(f, \theta) = \sum_i A_i(f, \theta) \exp\left(\frac{j4\pi f R_i(\theta)}{c}\right), \quad (1)$$

and where  $f$  is the radar frequency,  $\theta$  is the nominal aspect angle of the target, and  $c$  is the speed of light. The summation is over the apparent scattering centers on the target, which are located at reflection and diffraction points as well as at virtual points associated with multiple reflections and second-order diffraction. Each scattering center is characterized by its amplitude  $A_i$  and its effective range  $R_i$ . Table 1 shows the frequency dependence of  $A_i$  for some common scattering mechanisms, such as those typically found on the surfaces of satellites, reentry vehicles, and aircraft. In typical wideband-radar applications, the maximum bandwidth is approximately 10% of the center frequency, and the frequency variation of the scattering amplitude can be approximated by a low-order polynomial (e.g., by a Taylor series) about the center frequency.

The objective of radar imaging is to resolve the location of the scattering centers on the target. At a given aspect angle  $\theta$  of the target with respect to the radar line of sight, the scattering centers can be re-

**Table 1. Frequency Dependence of Amplitude  $A_i$  for Some Common Scattering Mechanisms**

Scattering Feature	Dependence ( $f^n$ ) $n$
Corner reflector	1
Flat-plate specular	1
Cylinder specular	1/2
Sphere or ellipsoid	0
Straight-edge specular	0
Cylinder base	-1/2
Cone tip	-1
Plate corner	-1

solved in range by measuring the radar cross section of the target over a band of frequencies. For each set of frequency measurements (i.e., each pulse), the frequency response of the target is converted to a range profile by the process of compressing the pulse (in most cases this process is a Fourier transform). The compressed pulse maps the scatterers on the target onto a line, referred to as the radar line of sight. The typical method used for digital pulse compression is to take the Fourier transform of Equation 1 with respect to  $f$  to produce the range profile  $s(r)$ . This method works because the different scattering centers manifest themselves as sinusoids in the spectral domain. The frequency of the sinusoid is proportional to the relative range of the scattering center.

The resulting range profile has a resolution (at points 6 dB down from the peak response) of

$$\delta r = \frac{c}{2b},$$

where  $b$  is the bandwidth of the radar. Even though we operate at the maximum achievable bandwidth of the radar, the range signature contains sidelobes that are only 13 dB down from the peak response. This result is an undesirable consequence of artificially truncating the frequency spectrum at the radar's bandwidth. The sidelobes can be reduced by weighting the frequency spectrum prior to the Fourier transform so that there is a smooth transition to zero at the edge of the spectrum. For example, the range resolution is degraded to  $1.81 \times \delta r$  with a Hamming weight, while the peak-to-sidelobe ratio is increased by 30 dB.

To form an image we also need to resolve the scattering center in a direction orthogonal to the range direction. The orthogonal direction to range is range rate, or Doppler. Resolution in Doppler can be achieved by collecting a series of pulses at different angles. A matched filter is constructed to map the position of scatterers in range as a function of the aspect angle  $\theta$  to a cross-range position [2, 3]. When the angular change is small, the matched filter can be derived by replacing each  $R_i(\theta)$  in Equation 1 with a two-term Taylor series. This substitution reduces the matched filter to a Fourier transform, and is identical to the range-resolution matched filter. As the aspect

angle  $\theta$  varies, sinusoids are formed in the measured data. Again, the frequency of the sinusoids is proportional to the Doppler displacement, or cross-range position of the scattering center. The resolution in the cross-range direction (at points 6 dB down from the peak response) is given by

$$\delta x = \frac{c}{2f_0 \Delta\theta},$$

where  $f_0$  is the center frequency and  $\Delta\theta$  is the angular change of the target observed by the radar.

In most cases the amplitude  $A_i$  as a function of aspect angle is well represented by a low-order Taylor series. In fact, most imaging algorithms are predicated on the amplitude remaining constant during the interval of image formation. In contrast to the range-resolution problem, there are situations in the aspect-angle direction in which a Taylor series is not a good representation of the amplitude. For example, in the special case when two scatterers interact in a flat-plate specular response, the amplitude functions of both scattering centers have the form

$$A(\theta) \approx \frac{1}{\theta - \theta_0}, \quad (2)$$

when the aspect angle  $\theta$  is well away from the specular at  $\theta_0$ . Away from the specular, Equation 2 can be approximated by a low-order Taylor series. As the aspect angle approaches the angle of the specular, the phases from the two scatterers begin to cancel and a sinc function is created.

#### *Bandwidth Extrapolation*

We can view the pulse-compression process as a spectral-estimation problem, where the spectrum to be estimated is the range profile. The traditional approach to spectral estimation is to use a nonparametric approach, such as the Fourier transform, to estimate the spectrum. Research in advanced spectral-estimation techniques, which has been ongoing since the late 1960s [8], has produced modern spectral-estimation techniques that are based on parametric modeling of the signal in the time, or range, domain. Typical parametric models include all-pole (or linear prediction), all-zero, and pole-zero models. Each of these models places different constraints on the data.

A frequency response that is expressed by Equation 1 can be approximated by a linear-prediction, or all-pole, model. The linear-prediction model for a uniformly sampled frequency spectrum, given by

$$v[n] = V(n\delta f, \theta), \quad (3)$$

states that the samples must meet the condition

$$v[n] = \begin{cases} -\sum_{i=1}^p a[i]v[n-i] & \text{forward} \\ -\sum_{i=1}^p a^*[i]v[n+i] & \text{backward,} \end{cases} \quad (4)$$

where  $\delta f$  is the frequency step between datum points,  $a[i]$  are the model coefficients, and  $p$  is the model order (which represents the number of scattering centers). This relationship holds when the number of scattering centers is known and the model coefficients are exact.

While numerous techniques exist for estimating coefficients of the linear-prediction model from measured data, this article considers only Burg's algorithm [8]. We have applied the other spectral-estimation techniques to radar data, but with limited success.

Burg's algorithm is an iterative procedure for determining coefficients that minimize the sum of the forward and backward prediction error over the entire data set. The prediction error is defined as the difference between the signal predicted by Equation 4 and the measured signal, given in the forward direction by

$$e^f = v[n] + \sum_{i=1}^p a[i]v[n-i],$$

and in the backward direction by

$$e^b = v[n-p] + \sum_{i=1}^p a^*[i]v[n-p+i].$$

The Burg algorithm is computationally efficient and yields a linear-prediction filter that is stable; i.e., the linear-prediction filter will not admit any exponentially growing signals. The stability of the filter is important. Other methods for estimating the coeffi-

cients, such as Prony's method and modified covariance, do not guarantee a stable filter. In our experience these other methods often fail with measured data, although they may perform better with ideal data.

Traditional parametric spectral-estimation techniques generate spectra analytically by using the magnitudes of the transforms of signal models derived from measured data. Given the model coefficients, the range profile is represented as

$$s(r) \propto \frac{1}{\left| 1 + a_1 e^{-j\tau} + \dots + a_p e^{-jp\tau} \right|}, \quad (5)$$

where  $r = c\tau/2$ . From the above expression, we can clearly see why Equation 4 is referred to as an all-pole model (see the appendix entitled "Spurious Scatterer Rejection in Bandwidth Extrapolation"). The location of the scattering centers is given by the zeros of the polynomial in the denominator.

A range profile produced in this way contains no phase information, and it has large variations of scattering-center locations and scattering amplitudes. In addition, the accuracy of the range profile depends completely on the accuracy of the signal model and

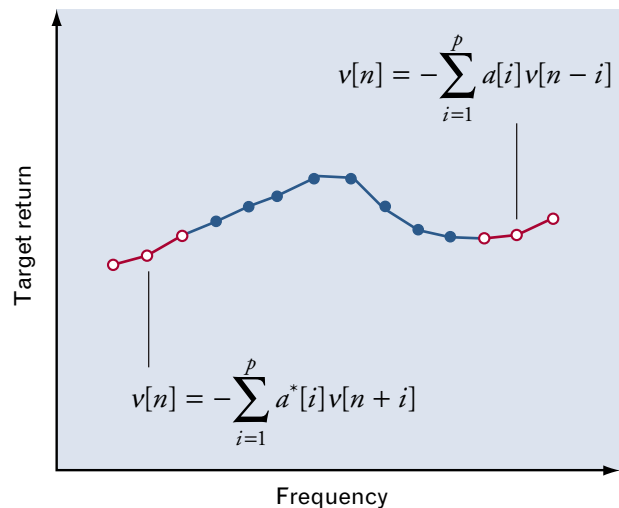


**FIGURE 1.** Bandwidth extrapolation. A linear-prediction model of the signal is combined with the measured radar data (in blue) to synthesize extrapolated data (in red) outside the measured bandwidth. The extrapolation for the higher frequencies is identical to the extrapolation for the lower frequencies, except for conjugated model coefficients.

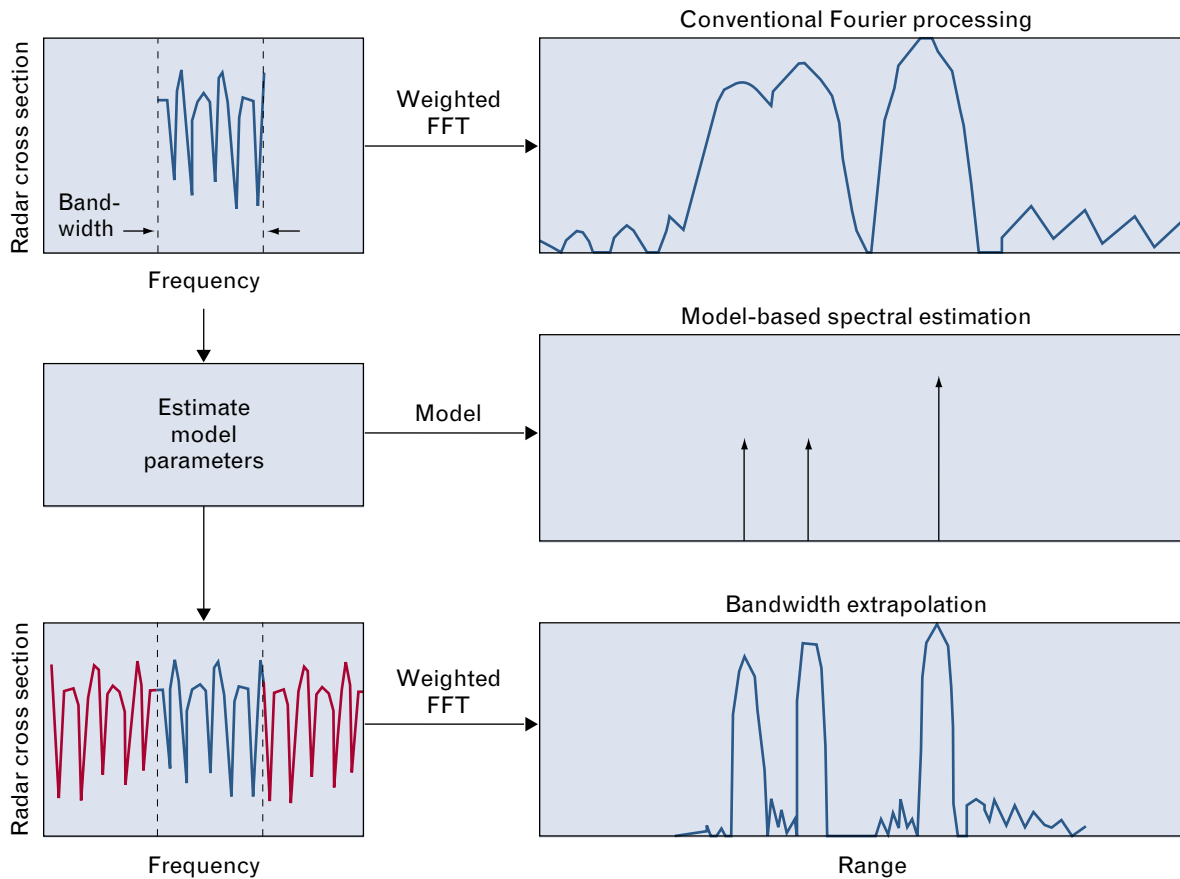


**FIGURE 2.** Comparison of spectral-estimation techniques, showing the conventional fast Fourier transform (FFT) processing method for pulse compression, the pure model-based spectral-estimation technique, and the bandwidth-extrapolation technique. The model-based technique provides the most information on scatterer position, while the bandwidth-extrapolation technique provides both scatterer-model data and stable amplitude data.

the estimation procedure. In the mid-1970s, however, Bowling proposed a technique that combined traditional parametric spectral estimation with the linear prediction of existing data [4], and formed the basis of bandwidth extrapolation.

The bandwidth-extrapolation algorithm proceeds as follows. Given frequency samples  $v[n]$ , Burg's algorithm is applied to the measured data to estimate the linear-prediction model coefficients  $a[i]$  by using an estimate of the model order  $p$ . The linear-prediction model is then used to extend the data outside the measured spectrum. The expansion is accomplished by using the signal model in Equation 3 and the measured signal data as initial conditions, as shown in Figure 1. The expanded pulse signal spectrum is then weighted and compressed via the Fourier transform.

Figure 2 illustrates the differences between conven-

tional Fourier spectral processing, parametric spectral-estimation techniques, and bandwidth extrapolation. The top row in the figure illustrates the limited range information available from conventional Fourier processing. The middle row depicts how the conventional model-based approach primarily yields scatterer position information. In contrast, the bottom row shows how a more conventional range profile is constructed by using an extrapolation approach and conventional Fourier processing.

Important features that contribute to the success of bandwidth extrapolation are the retention of measured data and the phase coherency of the resulting range signature. Another important feature is the use of conventional pulse compression after data expansion. The weighting process used in pulse compression reduces the influence of the extrapolated data on

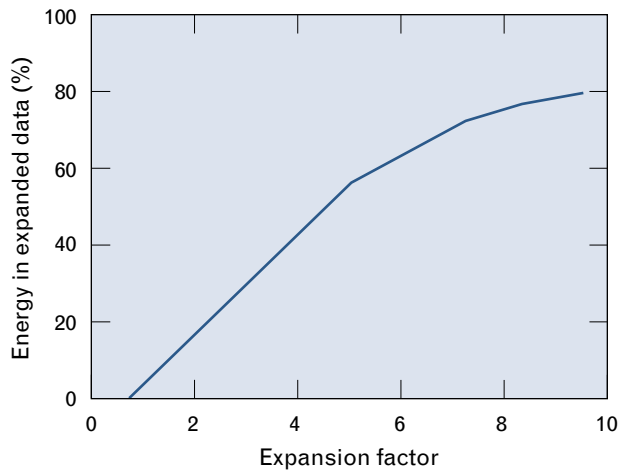


**FIGURE 3.** Energy in the extrapolated region. This curve represents the amount of energy in the synthetic extrapolated data, relative to the total energy in the range profile. For higher expansion factors (i.e., more synthetic data), the synthetic data contribute more to the range profile. Typically, expansion factors less than three lead to useful results.

the final range signature. Therefore, any errors in the extrapolated data are mitigated. This influence can be quantified in terms of the amount of energy that extrapolated data contribute to the range signature after the spectrum has been windowed. This contribution is estimated by calculating the amount of energy in the portion of the weighting window containing the extrapolated data. Figure 3 shows the energy content in the expanded portion of the data as a function of the ratio of the amount of extrapolated data to measured data when a Hamming weight is used for sidelobe reduction. This figure suggests that bandwidth expansions of more than three are significantly dependent on the accuracy of the expansion coefficient estimation.

For most cases the choice of model order  $p$  is not critical to the success of the technique. The model order is typically chosen to be one-third the number of data points present. This choice of model order leads to the largest number of coefficients that can be accurately estimated by the Burg algorithm. If these coefficients are used directly to produce a range signature, by using the analytic approach of Equation 5, a large number of spurious scatterers will be present. The spurious scatterers occur because the model order is determined from the number of data samples, and

not the physical properties of the target. The bandwidth-extrapolation algorithm naturally limits the spurious scatterers, as described in the appendix entitled “Spurious Scatterer Rejection in Bandwidth Extrapolation.”

#### *Aperture Extrapolation*

In contrast to bandwidth extrapolation, aperture extrapolation fixes the frequency and lets the aspect angle  $\theta$  vary. From the earlier discussion, the increase in the range of aspect angles leads to better resolution in the cross-range direction. From Equation 1 the sampled data are of the form

$$v[n] = V(f, n\delta\theta) = A_n \exp\left(j \frac{2\pi f R_n}{c}\right), \quad (6)$$

where  $R_n = R(n\delta\theta)$ ,  $A_n = A(f, n\delta\theta)$ , and  $\delta\theta$  is the aspect-angle increment between samples. The location of the scatterer in cross-range can be estimated by taking a Fourier transform of Equation 6 and scaling Doppler to cross-range. The primary difference between aperture extrapolation and bandwidth extrapolation is that phase may not be linear in  $n$  because of the scatterers’ complex range dependence on angle. For example, a simple rotating target causes  $R_n$  to have a sinusoidal dependence on  $n$ . When the phase dependence is linear in  $n$ , then the analysis proceeds exactly as in the range-resolution case. This is the case when the angle changes are small, and is assumed for the standard linear imaging [2].

Aperture extrapolation departs from bandwidth extrapolation in one other way. As we discussed previously, when the data to be extrapolated contain two scattering centers that cancel to form a specular response, the data are in the form of a sinc function. The sinc function does not meet the linear-prediction model. The Burg algorithm doesn’t fail in this case; it approximates the specular response by many point-scatterer responses. This approximation degrades the specular response in the image. The larger the extrapolated region, the more degradation is evident.

Figure 4 illustrates the result of applying aperture extrapolation to a typical specular response. The graphs on the left side of the figure show data and the correct Doppler response for a specular. The graphs on the right are the aperture-extrapolation results. In

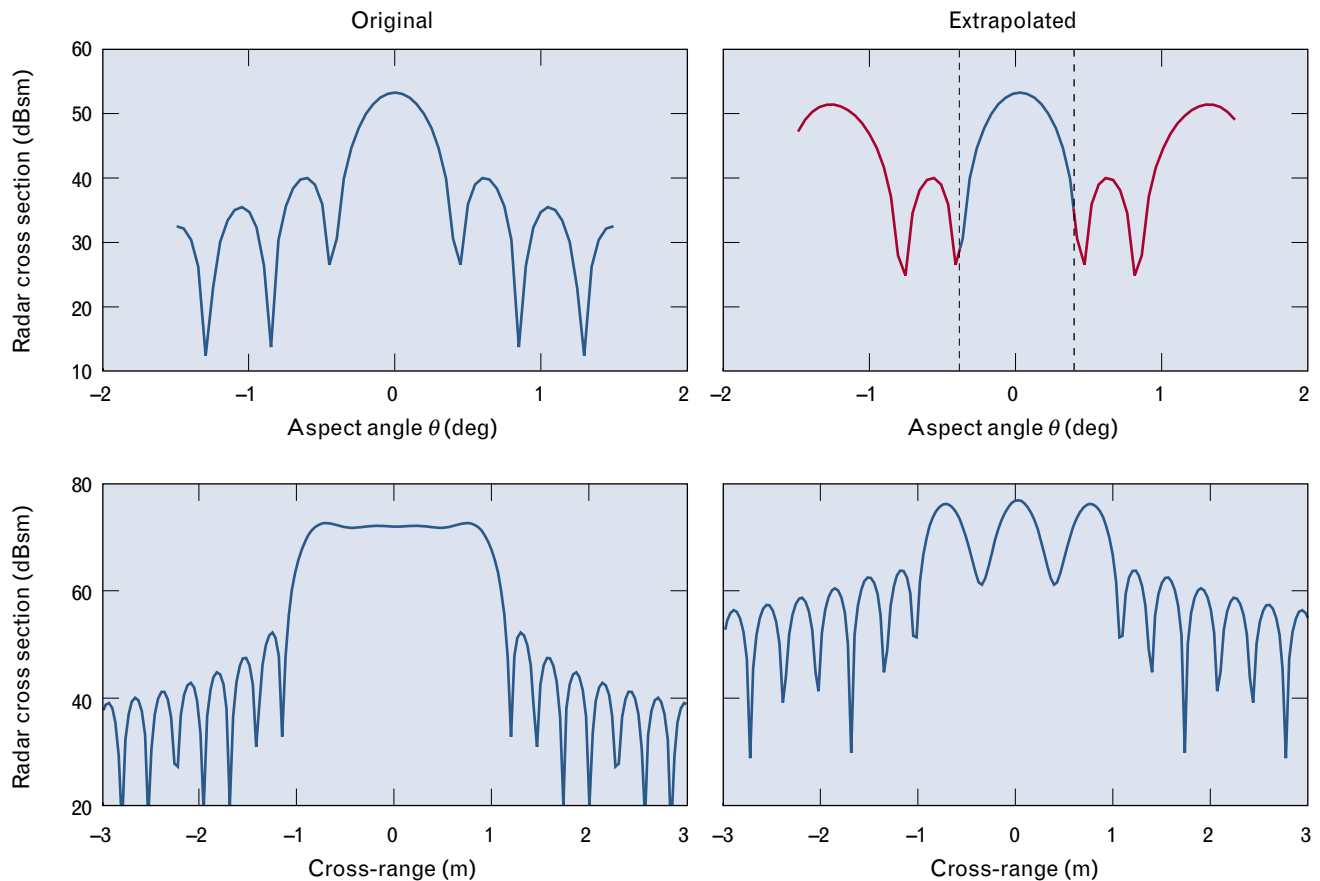


**FIGURE 4.** Aperture extrapolation of a specular response. The figure demonstrates what happens to a specular response when aperture extrapolation is used. Graphs on the left side of the figure show the original data, while graphs on the right side show the results of reducing the original data by four and applying aperture extrapolation. The red curve indicates the synthetic data. The degradation of the radar cross section, as shown in the graph in the lower right, is typical of what is seen in real images.

this example, the processing interval is chosen to be one-quarter the data collection interval, and therefore produces an expansion factor of four. The level of degradation of the radar cross section, as shown in the image on the lower right, is typical of what is seen in real images. The degradation increases if the initial interval does not contain the main lobe of the specular response. As a practical matter, the degradation of specular responses does not pose a serious problem because the occurrence of these phenomena is limited and the degradation typically does not affect image analysis.

Another difference from the range profile case is that the phase of a scatterer might not be linear with respect to  $n$ . It is typically the job of the imaging algorithm to interpret the nonlinear phase as the scatterers' position. If the linear imaging algorithm is used

(i.e., a Fourier transform), the nonlinear components will cause the image to appear blurred.

Within the limitations discussed in the above sections, aperture extrapolation can be used to produce a focused image from a blurred image while still using a linear image base algorithm. The procedure is first to reduce the data interval by a factor of two to four. This results in a more focused image, because the amount of contribution of the nonlinear phase is reduced, but the cross-range resolution is also reduced (recall that cross-range resolution is proportional to the total angular change). Then we apply aperture extrapolation to regain the lost resolution by using the previously described procedure.

Several issues must be understood before aperture extrapolation can be successfully applied to data with nonlinear phase. First, what form of phase depen-

dency will this method generate in the extrapolated data? And what will Burg's algorithm return for the coefficients in the linear-prediction model? In the remainder of this section we answer each of these questions.

The extrapolation of the data uses the linear-prediction model of Equation 4, with the measured data as the initial condition. The functional form of the model defines the types of signals that can be extrapolated. From the appendix entitled "Spurious Scatterer Rejection in Bandwidth Extrapolation" we know the class of functions that can be extrapolated are given by

$$p[n]z^n,$$

where  $p[n]$  is a polynomial in  $n$ , and  $z$  is a complex exponential function of the relative position of the scatterer. Because  $z$  is independent of  $n$ , any expansion that is performed generates data that have at most a linear phase variation, which is a necessary condition to produce a focused image.

A final question needs to be addressed. What coefficients will Burg's method generate for input data with a nonlinear phase? As an example, data with a quadratic phase are used. It is a straightforward procedure to substitute Equation 6 into Burg's algorithm and determine what the resulting model is for a single scatterer with a quadratic phase. Given that one scatterer is present and the model order  $p$  is chosen to be one, we can show that the coefficient produced by Burg's algorithm places the apparent location of the scatterer in the middle of the imaging interval. That is, the location of the scatterer is its average position during the imaging interval; we can also think of this process as linearizing the nonlinear function about the average angle.

### *Bandwidth Interpolation*

Signal interference is a major concern in processing radar imaging data collected over large bandwidths. Interfering signals often dominate the skin return of a target, and those portions of the signal bandwidth containing interference—even entire pulses—are blanked out. The resulting image is degraded because of frequency gaps in the range dimension or missing pulses in the cross-range dimension. The techniques

of bandwidth extrapolation, however, can be modified to reconstruct the notched-out (i.e., missing) signal components in a process we refer to as bandwidth interpolation.

For the purposes of explanation, we consider a signal with frequency notches, as shown in Figure 5. Here  $v[n]$  represents frequency samples of a target return, as shown in Equation 3, where  $n = 1, 2, \dots, N$ . (This technique works equally well with aperture extrapolation.) We assume that the signal has a single frequency notch; i.e., the data are missing from  $n = B$  to  $n = E$ , so that low-frequency data  $v_L[n]$  and high-frequency data  $v_H[n]$  are defined as

$$v_L[n] = \begin{cases} v[n] & \text{for } 1 \leq n < B \\ 0 & \text{elsewhere} \end{cases}$$

$$v_H[n] = \begin{cases} v[n] & \text{for } E < n \leq N \\ 0 & \text{elsewhere.} \end{cases}$$

Bandwidth-extrapolation algorithms could be applied directly to bandwidth interpolation where coefficients would be derived independently for the high-frequency and low-frequency data. In this case, two sets of data would be extrapolated (i.e., grown) into the notch,

$$v_L[n] = - \sum_{i=1}^{p_L} a_L[i] v_L[n-i] \quad (7)$$

for  $n = B, B+1, \dots, E$

$$v_H[n] = - \sum_{i=1}^{p_H} a_H^*[i] v_H[n+i] \quad (8)$$

for  $n = E, E-1, \dots, B$ .

The  $a_H$  coefficients and the  $a_L$  coefficients are Burg coefficients for high- and low-frequency data, respectively, and the constants  $p_H$  and  $p_L$  are Burg model orders for high- and low-frequency data, respectively. This representation leads immediately to an inconsistency. The number of scatterers in the extrapolated data will be different when the algorithm uses the coefficient derived from the high and low data, even though physically they should be the same. Data are

reconstructed in the notch by using a weighted sum of the extrapolated data,

$$\hat{v}[n] = \left( \frac{E-n}{E-B} \right) v_L[n] + \left( \frac{n-B}{E-B} \right) v_H[n], \quad (9)$$

where  $\hat{v}[n]$  are reconstructed data and  $B \leq n \leq E$ .

In addition to the previously mentioned model inconsistency, the direct application of bandwidth-extrapolation algorithms to bandwidth interpolation becomes less effective as notch widths increase and fewer data are available for calculating (i.e., estimating) the Burg coefficients. The resulting interpolated data are poorer approximations to the actual data in the frequency notch. These effects can be mitigated by combining high- and low-frequency data when we calculate the Burg coefficients, which is accomplished with minor modifications to the Burg algorithm.

As previously discussed, the Burg algorithm is an iterative procedure for calculating linear-prediction coefficients of a sampled signal. At each iteration, forward and backward prediction errors are used to calculate a reflection coefficient, which is then used to update prediction coefficients and prediction errors in subsequent iterations. At the  $l$ th iteration, the prediction errors used in these calculations are commonly given by

$$e_{l-1}^f[n] = v[n] + \sum_{i=1}^{l-1} a_{l-1}[i] v[n-i]$$

$$e_{l-1}^b[n-l] = v[n-l] + \sum_{i=1}^{l-1} a_{l-1}^*[i] v[n-l+i],$$

where  $e_{l-1}^f[n]$  is the forward prediction error,  $e_{l-1}^b[n-l]$  is the backward prediction error, and  $n = l+1, l+2, \dots, N$ . Equivalently, we can view  $e_{l-1}^f[n]$  and  $e_{l-1}^b[n-l]$  at each iteration as coming from a computation window that extends from  $n-l$  to  $n$ . The Burg algorithm can be modified to omit those prediction error calculations when any portion of the computation window falls within the frequency notch. The result is a single set of Burg coefficients  $a[i]$  that are derived from data at all frequencies. The notch is then filled by extrapolating the signal from both sides, similar to Equations 7 to 9 above.

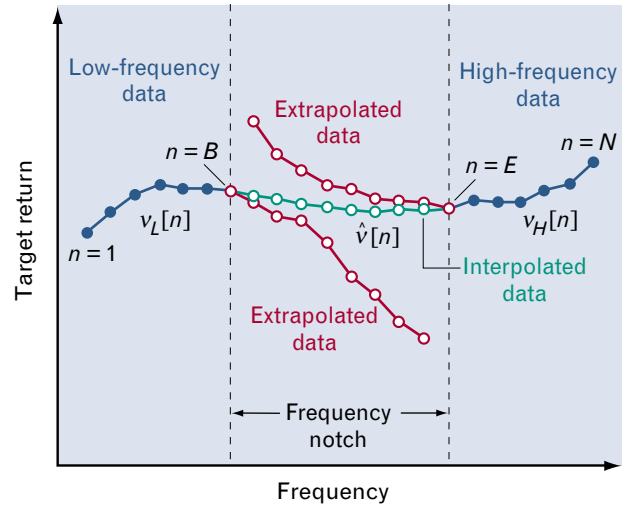


**FIGURE 5.** Bandwidth interpolation. The technique of bandwidth extrapolation can be modified to reconstruct missing signal components. Bandwidth extrapolation is used in the frequency notch to generate synthetic data (in red) from the low-frequency data and the high-frequency data (in blue). The interpolated synthetic data (in green) are then produced from a weighted sum of the extrapolated data.

## Examples

This section of the article applies the techniques of bandwidth extrapolation, aperture extrapolation, and bandwidth interpolation to measured wideband data on aircraft. Because the performance of the algorithm can be better observed by looking at individual signatures, we begin by looking at range signatures. We then apply the data to ISAR imagery of a small commercial aircraft.

### Range Signatures

We begin by illustrating the performance of bandwidth extrapolation on a complex target. A signature was selected from a database of measured aircraft signatures and reduced in bandwidth by factors of two and four, with the resulting signatures shown in Figure 6. In the first case the signature with the quarter bandwidth was enhanced back to half the original bandwidth. The second case extrapolated the quarter-bandwidth signature back to the original bandwidth. In each case the number of coefficients in the model was chosen to be one-third the number of data points after the bandwidth reduction. Because the full-resolution signature has 390 points, the half-bandwidth

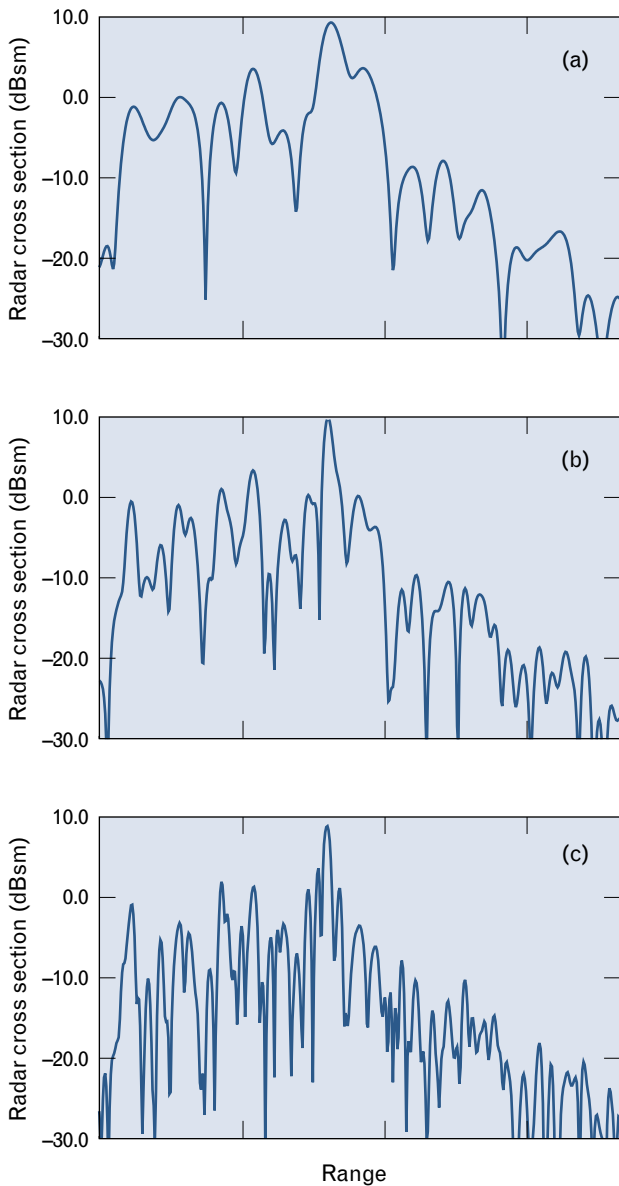


**FIGURE 6.** High-resolution range profiles of an aircraft at three different bandwidths: (a) one quarter, (b) one half, and (c) full.

signature has 195 points, and the quarter-resolution signature has 97 points. As mentioned earlier, the one-third rule represents a balance between the accuracy of the coefficient estimation and having as large a model as possible.

Figures 7 and 8 compare two-to-one and four-to-one extrapolated signatures to the original signature. The result of extrapolation by a factor of two, shown in Figure 7, demonstrates the similarity of the extrapolated-bandwidth signature to the original signa-

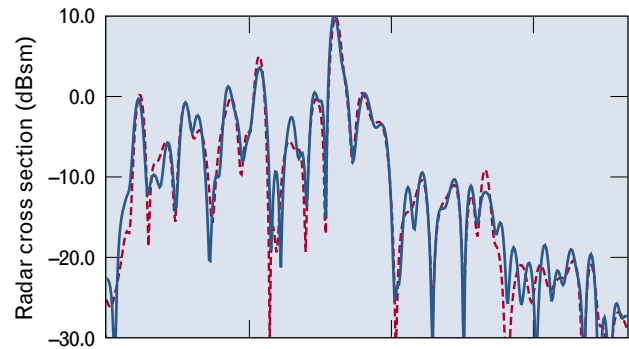


**FIGURE 7.** Comparison between a two-to-one extrapolated signature (red dashed line) and the measured half-bandwidth signature shown in Figure 6(b). The extrapolated half-bandwidth signature was formed from the measured quarter-bandwidth signature in Figure 6(a).

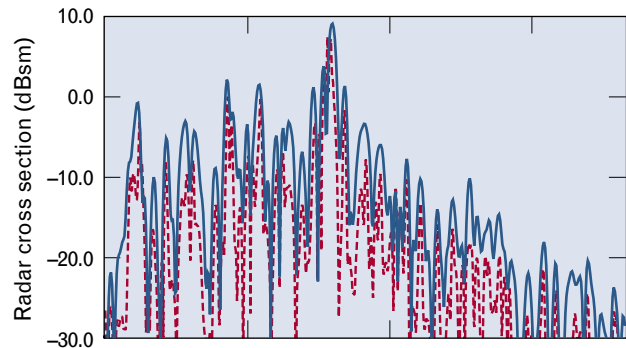


**FIGURE 8.** Comparison between a four-to-one extrapolated signature (red dashed line) and the measured full-bandwidth signature in Figure 6(c). The extrapolated full-bandwidth signature was formed from the measured quarter-bandwidth signature in Figure 6(a).

ture. Note that although the model order was chosen to be thirty-two there are fewer than thirty-two scatters present in the signature. Figure 8 shows that a four-to-one extrapolation does not provide as good a quality of match. This reduced performance has several sources. Not only do the extrapolated data have a greater relative influence compared to the measured data for larger expansion factors, but we expect the accuracy of the extrapolated data at the ends to degrade as the expansion factor increases. In addition, the accuracy of the coefficients is degraded because there are fewer data points to estimate the coefficients. Perhaps more importantly, we must use a lower model order that may not be large enough to capture the complexity of the signature.

The previous example used only one signature. To

**Table 2. Correlation Coefficients for Various Extrapolations**

<i>Extrapolation</i>	<i>Mean</i>	<i>Median</i>	<i>Standard Deviation</i>
× 2	0.972	0.973	0.00951
× 3	0.896	0.898	0.0266
× 4	0.803	0.807	0.0501

better quantify performance we examined a set of six hundred signatures whose resolutions were degraded and then improved by using the bandwidth-extrapolation technique. In order to assess the performance of the bandwidth-extrapolation algorithm, we correlated the original signature with the extrapolated signature, and recorded the peak correlation response. Table 2 gives the results of this numerical experiment.

The data in this table clearly indicate that the larger the extrapolated region, the more the extrapolated range profile differs from the original. This result does not indicate that larger extrapolations are not useful. The same signatures were also fed into an identification algorithm, which is designed to identify the type of aircraft from the wideband range profile. When the bandwidth-extrapolated data were fed into the identification algorithm, which had been trained on measured data, there was a significant loss in performance. In contrast, when the identification algorithm was trained to expect extrapolated data, the measured data needed only one-fourth the bandwidth to achieve the same level of correct identification. In addition, there was no increase in the number of false alarms detected with the bandwidth-extrapolated data over the measured data. This result clearly indicates that the usefulness of any algorithm is dependent on the individual application involved.

#### *Aircraft Imaging Examples*

In May 1995, the Navy NRaD X-band radar [9] collected image data on a small commercial aircraft. The radar used an LFM waveform with an instantaneous bandwidth of 500 MHz and a pulse repetition frequency of 150 Hz. The target aircraft flew in a circu-

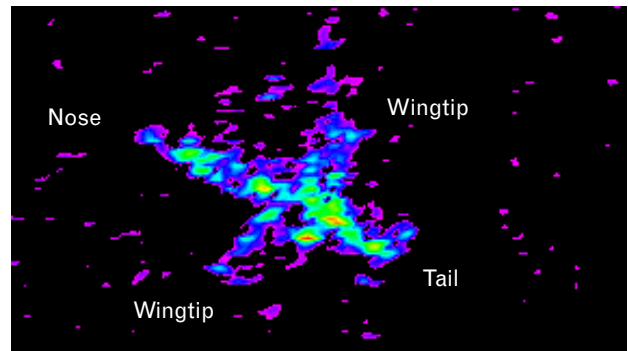


**FIGURE 9.** Range-Doppler image of a small commercial aircraft at full-bandwidth resolution and integration time. The strongest radar scatterers are along the length of the fuselage, with weaker scatterers across the wing span and in the tail.

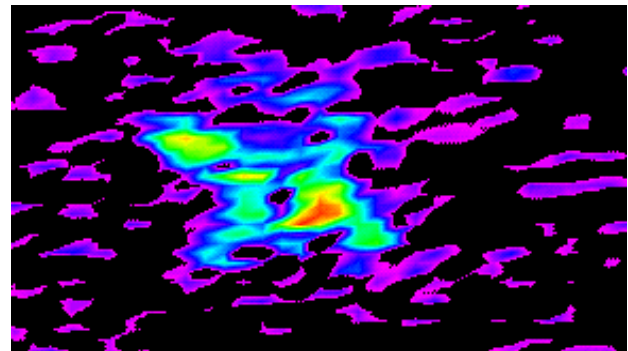


**FIGURE 10.** Range-Doppler image of a small commercial aircraft, reduced in bandwidth and integration time by a factor of three. The lower resolution degrades the image in both range and cross-range, which increases the uncertainty in locating the scatterers along the aircraft fuselage and across the wing span.

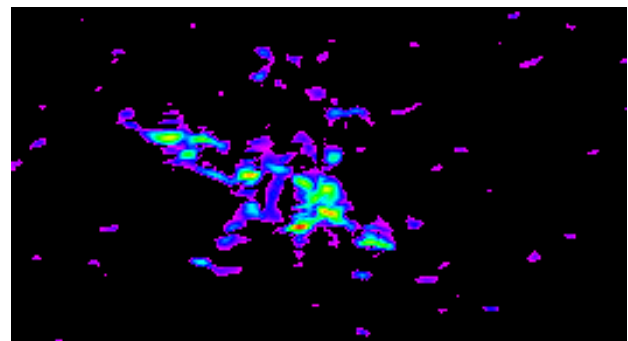


**FIGURE 11.** Restored range-Doppler image of a small commercial aircraft, produced by applying bandwidth extrapolation and aperture extrapolation to the reduced-resolution image in Figure 10. This enhanced image is comparable to the image in Figure 9 in both resolution and in the position of the strong scatterers.

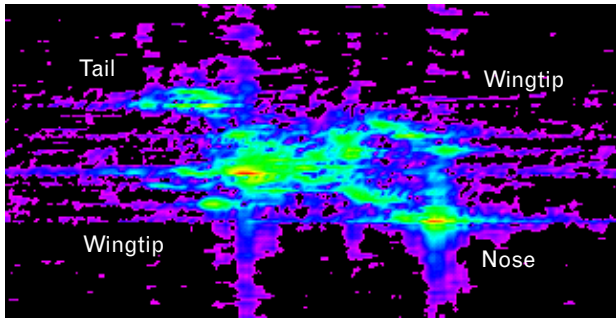


**FIGURE 12.** Degraded image of a commercial aircraft with 40% of the pulses missing in the data. The missing pulses increase the Doppler sidelobe levels, creating an image with broad cross-range response and degraded cross-range resolution.

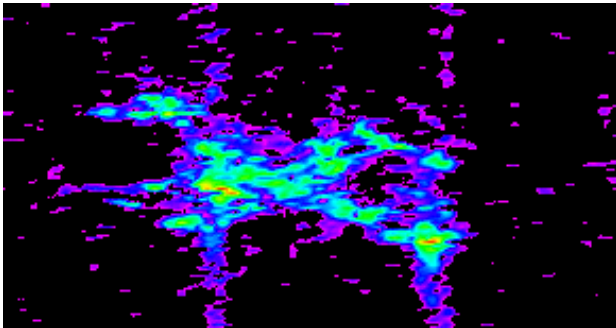


**FIGURE 13.** Restored image of a commercial aircraft with the missing pulses filled by bandwidth interpolation. The cross-range resolution of the strong scatterers is clearly improved.

lar flight path at a turn rate of approximately three degrees per second. Figure 9 shows a full-resolution image formed by using a one-second integration time. The Lincoln Laboratory range-Doppler smoothing algorithm was used for motion compensation (see the appendix entitled “Imaging Algorithm for Aircraft in Flight”). In Figure 9, the nose of the aircraft is pointed toward the upper left, while the wing tips are pointed toward the upper right and lower left. The image shows the strongest radar scatterers along the length of the fuselage, with weaker scatterers across the wing span and in the tail.

Existing multifunction radars have been considered for producing images of tactical aircraft in flight. Typically, these radars have limited bandwidths and do not support long uninterrupted integration times for imaging. Figure 10 shows the identical image data of Figure 9, but with bandwidth and integration time

reduced by a factor of three. The image is degraded in both range and cross-range, which increases the uncertainty in locating the scatterers along the aircraft fuselage and wing span. Both bandwidth extrapolation and aperture extrapolation were applied to the low-resolution data of Figure 10 to enhance the image back to the original resolution. Figure 11 shows the results of the resolution enhancement. The original image in Figure 9 and the enhanced image in Figure 11 are comparable in resolution as well as in the position of the strong scatterers.

Another approach to imaging with short integration times is to coherently combine and process data from separate processing intervals, or dwells. This technique produces an image dwell with missing pulses. Figure 12 shows an image from a dwell with missing data, where the middle 40% of the pulses in the imaging interval are missing. The missing data increase the Doppler sidelobe levels, creating an image

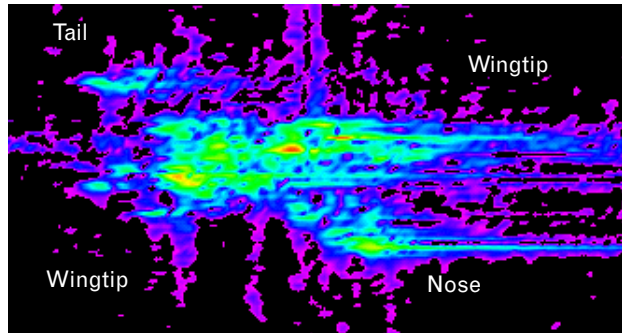


**FIGURE 14.** Defocused image of a commercial aircraft because of insufficient motion compensation. The lack of motion compensation produces the Doppler streaks in the right side of the image.

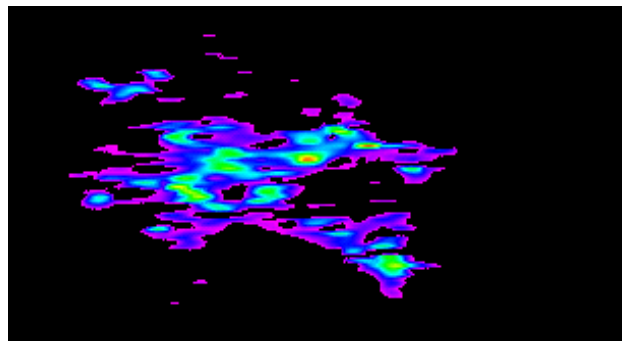


**FIGURE 15.** Improved focused image because of aperture extrapolation. The Doppler streaks shown in Figure 14 are eliminated.

with broad cross-range response and degraded cross-range resolution. Bandwidth interpolation can be used to interpolate the missing data and restore image resolution. Figure 13 shows the result of applying bandwidth interpolation to the degraded data of Figure 12. The cross-range resolution of the strong scatterers is clearly improved in the restored image.

Aircraft maneuvers or rapid acceleration may lead to instances in which the range-Doppler smoothing algorithm cannot model the motion of the target. Figure 14 shows a blurred image from the pass of the commercial aircraft. Motion compensation did not properly account for aircraft motion, giving rise to the Doppler streaks shown on the right side of the image. In this case, aperture extrapolation can be used to produce a focused image. The imaging interval is cut down by a factor of three, producing a low-resolution image, and aperture extrapolation is used to restore the original resolution. Figure 15 shows the results of this process, in which image focusing is improved and the Doppler streaks are eliminated.

### Summary

In this article we have described a powerful set of robust, model-based techniques that can be used in a variety of ways to improve the quality of ISAR images. Resolution can routinely be improved in both range and cross-range by a factor of two or more, and data that might otherwise be of little use for imaging can be repaired to yield high-quality images.

The key theoretical foundation for this approach is the introduction of a general underlying model for target scattering. This model is consistent with high-frequency scattering from complex targets. In this article several distinct applications of this approach have been demonstrated. The general concept is to use the model, together with the measured data, to estimate values for the target return in which valid measurements are not available. This estimation can extend the measurement region (extrapolation) or it can fill in where data are missing (interpolation).

For extrapolation we have discussed how bandwidth extrapolation can be used to increase the effective resolution of individual pulses, thus improving the resolution in the range domain as well as increasing noncooperative target identification. A similar ap-

proach was used to extend the effective integration time (aspect-angle change), thus improving the resolution in Doppler (cross-range).

We have applied extensions of these extrapolation methods for interpolation. They have been used to estimate the target return over a band of frequencies that were missing from within the overall bandwidth of the waveform (perhaps caused by in-band interference), and they have been used to reconstruct pulses that were missing within a data collection interval.

### Acknowledgments

The authors would like to thank Dennis Andersh, Walt Barnes, Tom Morton, and Rett Wisman for their support of these efforts. This work was sponsored by the U.S. Air Force.

---

## REFERENCES

1. Wright Laboratory, Wright-Patterson AFB, branches AARA and AARM (currently branches AAMR and AACT).
2. D.A. Ausherman, A. Kozma, J.L. Walker, H.M. Jones, and E.C. Poggio, "Developments in Radar Imaging," *IEEE Trans. Aerosp. Electron. Syst.* **20** (4), 1984, pp. 363-400.
3. T.G. Moore, "A New Algorithm for the Formation of ISAR Images," *IEEE Trans. Aerosp. Electron. Syst.* **32** (2), 1996, pp. 714-721.
4. S.B. Bowling, "Linear Prediction and Maximum Entropy Spectral Analysis for Radar Applications," *Project Report RMP-122*, Lincoln Laboratory (24 May 1977), DTIC #ADA-042817.
5. K.M. Cuomo, "A Bandwidth Extrapolation Technique for Improved Range Resolution of Coherent Radar Data," *Project Report CJP-60, Rev. 1*, Lincoln Laboratory (4 Dec. 1992), DTIC #ADA-258462.
6. E.C. Burt, T.G. Moore, and B.W. Zuerndorfer, "Enhanced Resolution Imagery from Limited Data," *NATO AC/243 (Panel 10/RSG 12) Workshop on Radar Imaging and Classification Techniques, Wachtberg-Werthhoven, Germany, 28-29 Jan. 1993*, pp. 4.1-4.19.
7. E.C. Burt, T.G. Moore, and B.W. Zuerndorfer, "Auto-Focusing of Moving Targets," *NATO AC/243 (Panel 10/RSG 12) Workshop on Radar Imaging and Classification Techniques, Wachtberg-Werthhoven, Germany, 28-29 Jan. 1993*, pp. 5.1-5.21.
8. S.M. Kay, *Modern Spectral Estimation, Theory and Applications* (Prentice-Hall, Englewood Cliffs, N.J., 1988).
9. J. Trischman, S. Jones, R. Bloomfield, E. Nelson, and R. Dinger, "An X-Band Linear Frequency Modulated Radar for Dynamic Aircraft Imaging," *Proc. 16th Annual Symp. of Antenna Measurement Techniques Assoc., Long Beach, Calif., 3-7 Oct. 1994*, pp. 431-436.

## APPENDIX A: SPURIOUS SCATTERER REJECTION IN BANDWIDTH EXTRAPOLATION

ONE OF THE PRACTICAL features of bandwidth extrapolation is the reduction in the number of spurious scatterers from estimated model coefficients in the extrapolated data. The reduction of the spurious scatterers can be understood by casting the extrapolation part of the algorithm as a difference equation.

After the Burg algorithm has been performed we are left with an equation of the form

$$v[n] + \sum_{i=1}^p a[i]v[n-i] = 0, \quad (1)$$

which is a constant-coefficient difference equation. The class of solutions admitted by Equation 1 are of the form

$$v[n] = \sum_i C_i P[n] z_i^n, \quad (2)$$

where  $C_i$  is a constant,  $P[n]$  is a polynomial in  $n$ , and  $z_i$  is the solution to the characteristic equation

$$1 + \sum_{i=1}^p a[i]z^i = 0. \quad (3)$$

The summation in Equation 2 is over the number of distinct roots of Equation 3. The order of the polynomial  $P[n]$  is governed by the number of duplicate roots of the characteristic polynomial. In practice the roots correspond to scatterer location; i.e.,

$$z^i = e^{j(4\pi f_0 R_i/c)\delta f},$$

where  $f_0$  is the radar center frequency,  $R_i$  is the scatterer location, and the constants  $C_i$  in Equation 2 correspond to the scatterers' amplitude.

If we continue the analogy of the difference equation, the next step is to find the unknown coefficients  $C_i$ . This is done by using the measured data as initial conditions, which leads to a set of linear equations for the unknowns. If the measured data have fewer scatterers present than the model order  $p$ , the initial conditions will throw out extraneous solutions and the extrapolation process will generate a signal only for the scatterers that are present.

---

---

## APPENDIX B: IMAGING ALGORITHM FOR AIRCRAFT IN FLIGHT

UNCOMPENSATED TRANSLATIONAL motion is one of the principal limitations in our ability to focus radar images of aircraft. The range-Doppler smoothing (RDS) technique was developed from autofocusing of satellite imagery; it compensates high-order translational motion of aircraft to yield well-focused images. Because RDS does not explicitly address rotational motion of the target, the cross-range scaling of the resulting imagery is uncalibrated. However, close cou-

pling between rotational and translational motion for coordinated aircraft flight allows cross-range scaling to be derived by extending RDS processing to azimuth and elevation data. The principal assumption of RDS is that airborne target position is a smooth function of time.

The ideal first step in compensating the translational motion of a target aircraft is to determine the range to the same scatterer on the target at every

pulse. Generally, this range determination is not possible because aircraft motion prevents the same scatterer from being visible at every pulse. Also, low signal-to-noise levels at long ranges as well as interference between scatterers can obscure individual scatterers on a given pulse.

Instead, RDS finds the range to the same area on the target at every pulse. This is done by median-processing each pulse to estimate the range to the center of the target. The center of the target is used because it is relatively free of scattering from moving parts of the aircraft. For example, scattering from rotating engine blades often occurs toward the rear of the aircraft, while scattering from scanning antennas occurs toward the front of the aircraft. The output of median processing can vary by a range gate or more from pulse to pulse and produce jitter in the range estimates. Because of the smooth motion of the target, these range estimates are improved by using a least-squares fit to a smooth function of time. Typically, the functions are high-order polynomials.

These range polynomials are evaluated at the transmit time of each pulse to form a smoothed estimate of the range to the target center for each pulse. Such smooth range estimates are used to align each pulse in range. Once these aligned pulses are processed into images, the target image will be centered in range but may drift in cross-range and may not be consistently focused. The drifting occurs because of small differences between the actual range and the estimated range to the target; these differences can be on the order of a few wavelengths. Doppler processing is required to compensate this fine residual motion.

Fine motion compensation is performed by using the signal at the center range gate of each pulse. In the ideal case, this range gate is dominated by a single scatterer, so the signal amplitude represents the strength of the scatterer and the signal phase represents its range. This suggests it is possible to compensate the fine motion of the target by using this signal phase directly, but not without difficulty. There may be more than one scatterer at the center range gate, or a strong scatterer may walk out of the center range gate. Alternatively, the change in phase as a function of time (i.e., the Doppler frequency) of the center range gate can be integrated to yield the signal phase

necessary to compensate the fine motion of the target.

In RDS Doppler processing, the complex signal is recorded at the center range gate of each pulse. With a constant pulse repetition frequency, these signal values are Fourier transformed to yield the Doppler distribution of the scatterers in this range gate within an integration interval. The integration interval is sufficiently short so that the same scatterers are present throughout the interval; i.e., the scattering is coherent over the integration interval. The integration interval is updated with each pulse to give Doppler distributions as a function of time.

These distributions tend to be well centered, and a centroid is used to estimate the center Doppler frequency of each distribution. Occurrences of broad Doppler responses, such as specular flashes, and the effects of noise can create jumps in the Doppler estimate. Thus target Doppler is tracked and smoothed as a function of time by using a polynomial fit to the Doppler estimates, which is similar to the process used for range alignment. A smooth estimate of Doppler is formed by evaluating the polynomial at the transmit time of each pulse. Integrating the Doppler polynomial over time yields the phase of the target return.

Once the range and Doppler polynomials have been determined, focused images are produced by (1) aligning each pulse in range by using the smoothed range estimates from range processing, (2) phase-shifting each data pulse by the combined phase from range and Doppler processing, and (3) using the fast Fourier transform to form linear images.



**THOMAS G. MOORE** is a former senior staff member in the Radar Imaging Techniques group, where he conducted research in the areas of radar imaging, signal processing, and computational electromagnetics. He received B.S., M.S., and Ph.D. degrees in electrical engineering from Northwestern University.



**BRIAN W. ZUERNDORFER** is a staff member in the Radar Systems group. His current areas of research are in combat identification, noncooperative target recognition, target parameter estimation, and signal processing. Prior to joining Lincoln Laboratory in 1992, he worked at RCA Corporation, MITRE, and Raytheon. He received B.S. and M.E. degrees in biomedical engineering from Rensselaer Polytechnic Institute, and a Ph.D. degree in electrical engineering from the University of Michigan. In 1995 he received an award for the best technical presentation at the Joint Service Combat Identification Systems Conference. He is a member of Sigma Xi and Tau Beta Pi



**EARL C. BURT** is a senior staff member at the Kwajalein radar measurements field site, in the Republic of the Marshall Islands, where he conducts research in electromagnetic scattering and radar signal processing. He received a B.S. degree in physics from St. Lawrence University, and M.S. and Ph.D. degrees in mathematics from Syracuse University. Before joining Lincoln Laboratory in 1986, he was employed by the Syracuse Research Corporation. He is a member of the Electromagnetics Academy and a senior member of the IEEE.